Calibration of the AGILE Gamma Ray Imaging Detector

Andrew Chen on behalf of the AGILE Team

April 11, 2011

AGILE

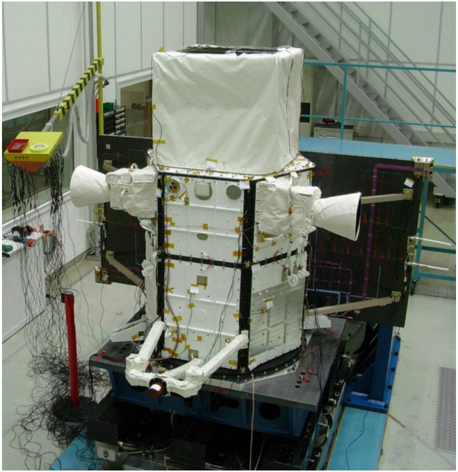

- Astrorivelatore Gamma ad Immagini LEggero
- Italian Space Agency (ASI) small mission
- Participation from INAF, INFN, Italian univerities, industrial partners
- Launched April 23, 2007 from Sriharikota, India

AGILE

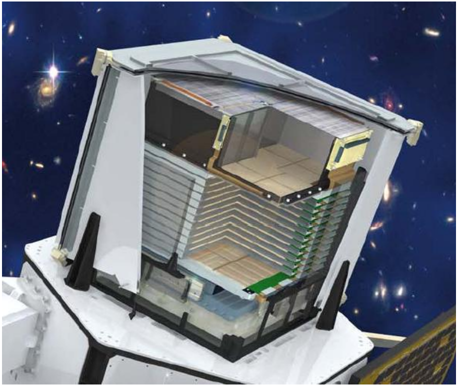

- Gamma-ray Imaging Detector (GRID): 30 MeV - 50 GeV
- X-ray detector (Super-AGILE): 18-60 keV
- Mini-calorimeter (MCAL): 300 keV - 100 MeV

AGILE-GRID

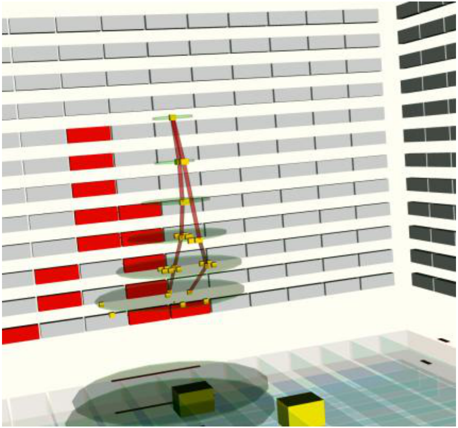

- Pair-production telescope
- Tungsten-Silicon Tracker: 12 planes, $0.8X_0$
- $38.06 \times 38.06 \times 21.078$ cm^3

On-board Trigger

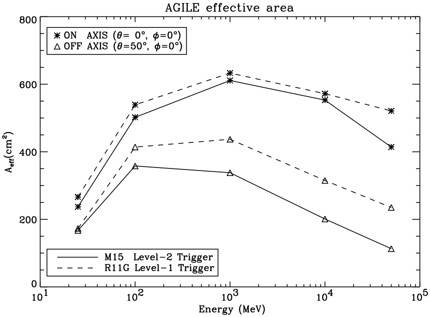

- Combination of hardware (Level-1) and software (Level 2)
- Simulations in GEANT v3.21
- Validated with cosmic-ray muons at Tortona and beam tests at INFN-Frascati

Event reconstruction - Kalman filter

- Simplified on-board Kalman filter to reject albedo photons
  - Retains 85-95%
- On-ground analysis using complete Kalman filter
- Provides reconstructed energy and photon incidence direction
- Unreconstructable events are rejected

Background rejection filters

- Detailed analysis of event morphology to distinguish photons from charged particles
- Events classified as gamma-rays (G), uncertain (L), particles (P) or single-track (S)
- All analysis except pulsar timing use G exclusively

Monte Carlo Simulations

- Series of runs with 59×10^6 events each over a radius of 136.5 cm
- Spectral index -1.7, energies ranging from 4 MeV to 50 GeV
- Each run contains a parallel plane of photons from a different incidence direction
- Off-axis angle $= 1,30,35,40,45,50,60^\circ$
- Roll angle 0, 45°

Effective area

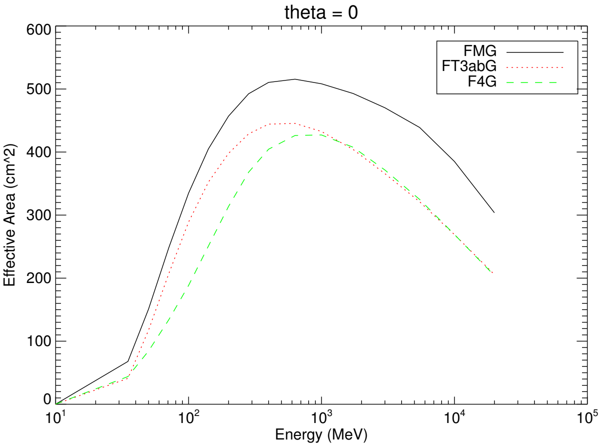

Figure: geometric area × fraction of surviving events classified as G

Effective area

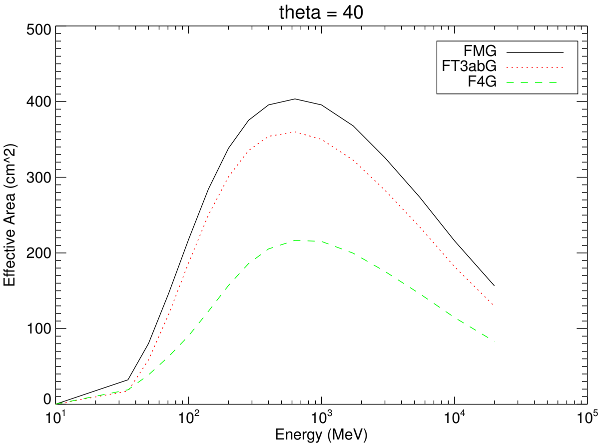

Figure: geometric area × fraction of surviving events classified as G

Energy Dispersion

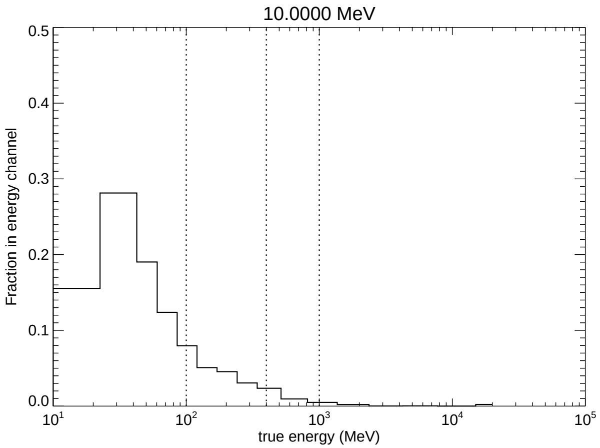

Energy Dispersion

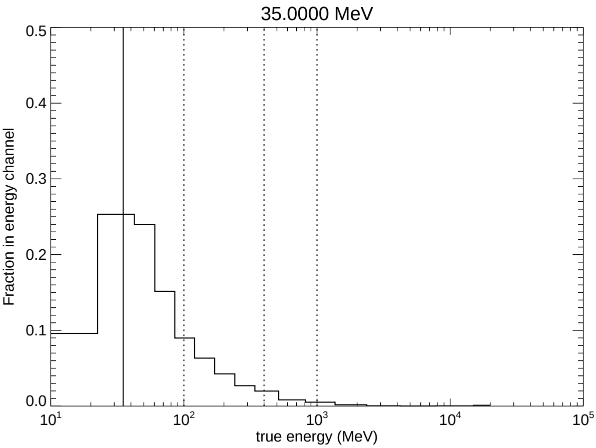

Energy Dispersion

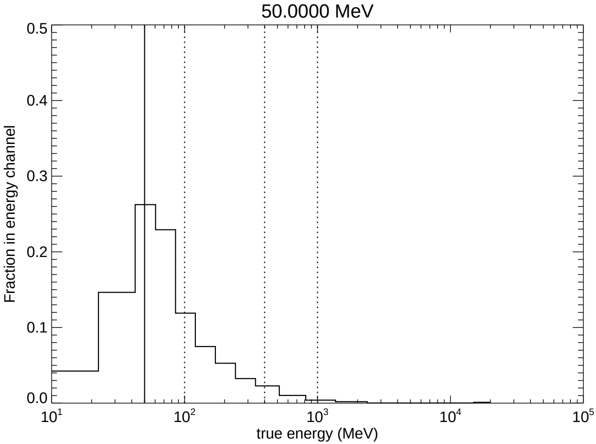

Energy Dispersion

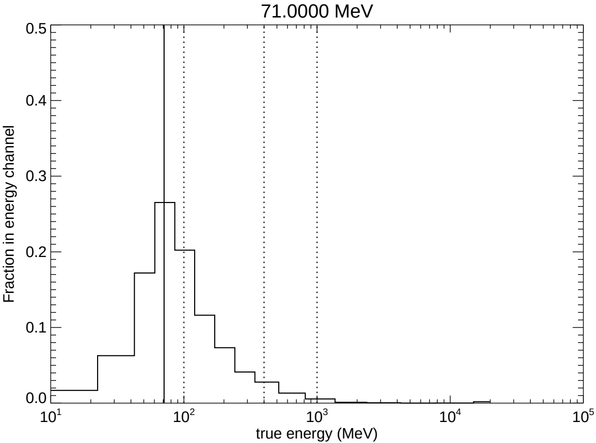

Energy Dispersion

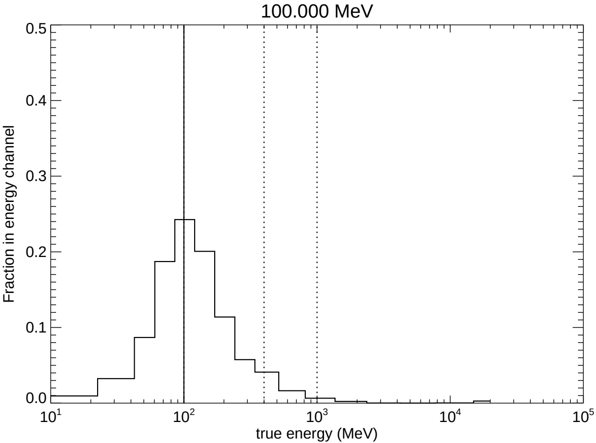

Energy Dispersion

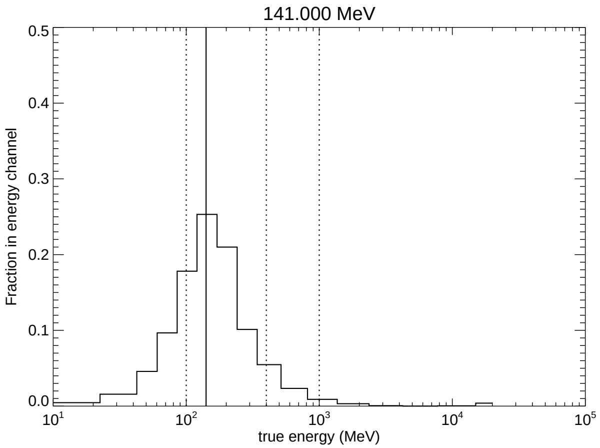

Energy Dispersion

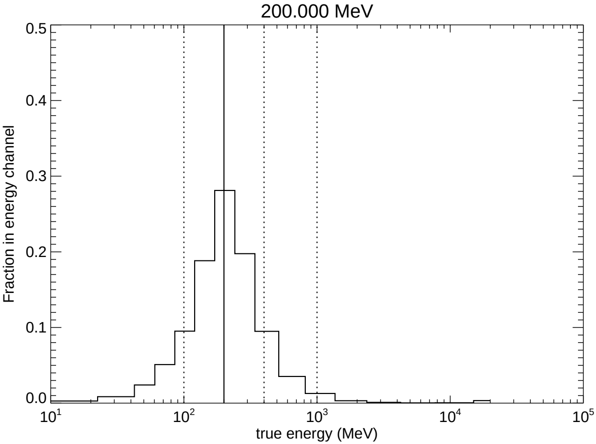

Energy Dispersion

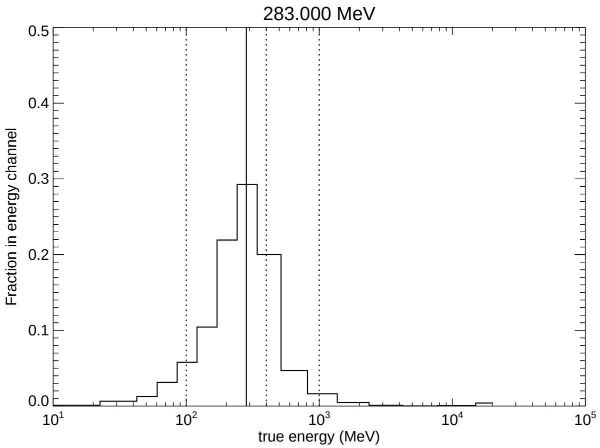

Energy Dispersion

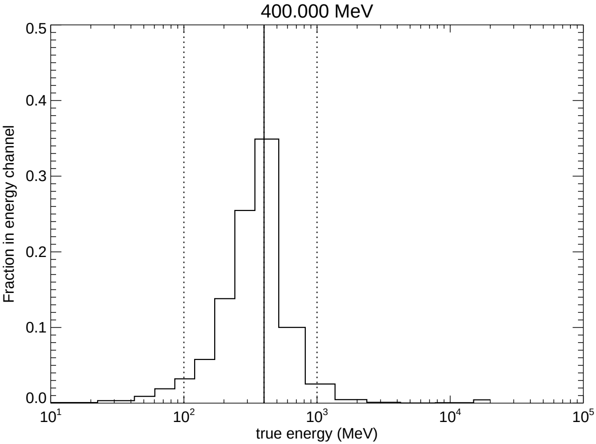

Energy Dispersion

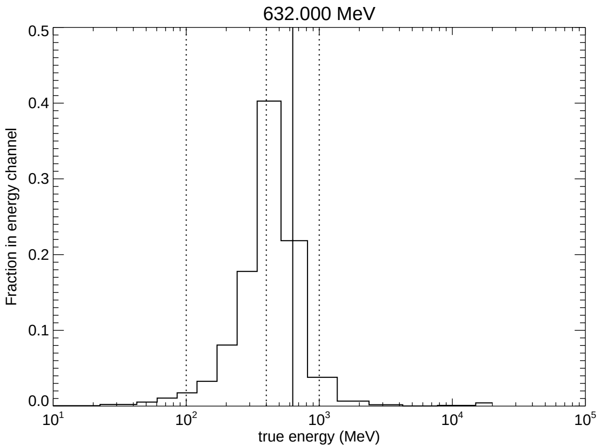

Energy Dispersion

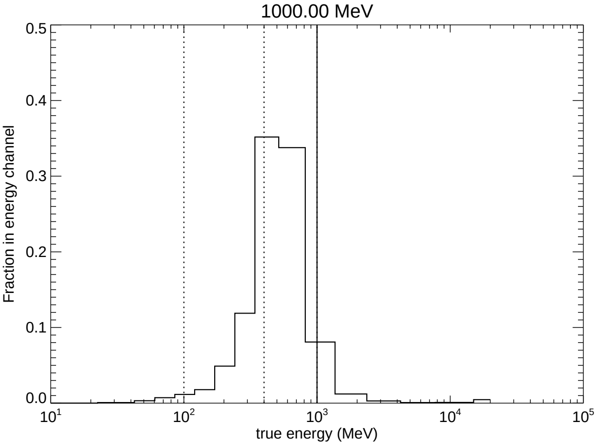

Energy Dispersion

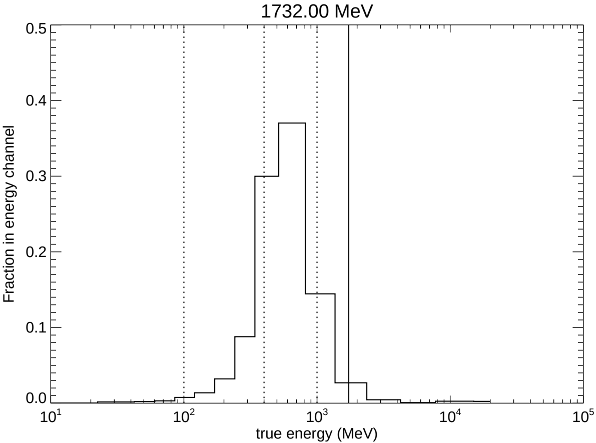

Energy Dispersion

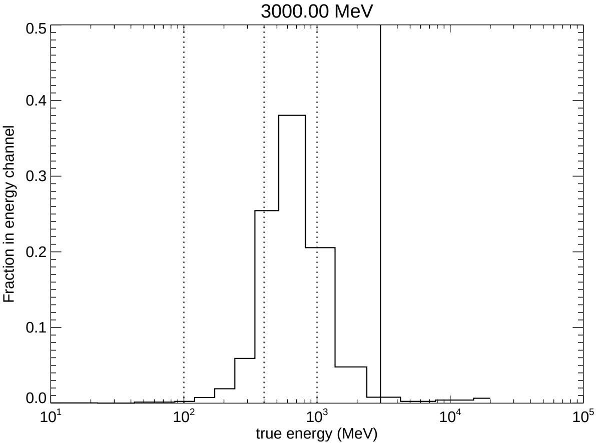

Energy Dispersion

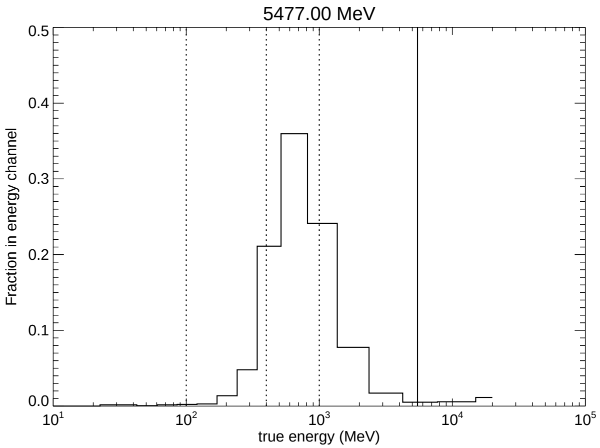

Energy Dispersion

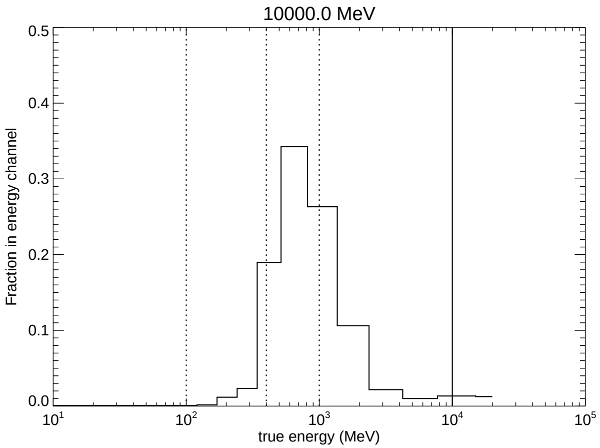

Energy Dispersion

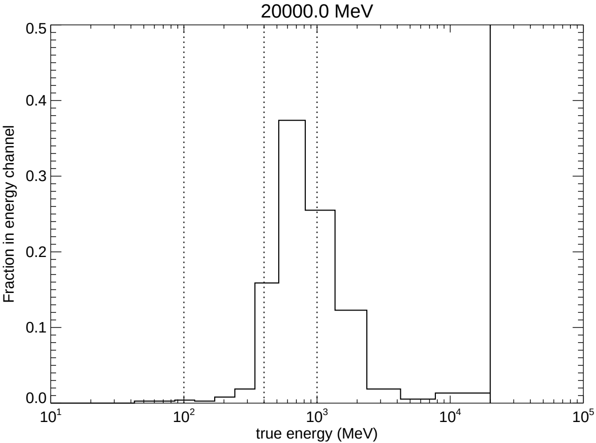

Point spread dispersion

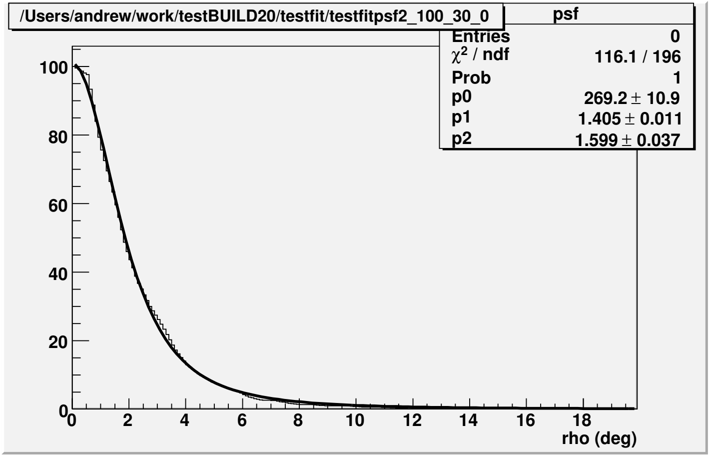

Point spread dispersion

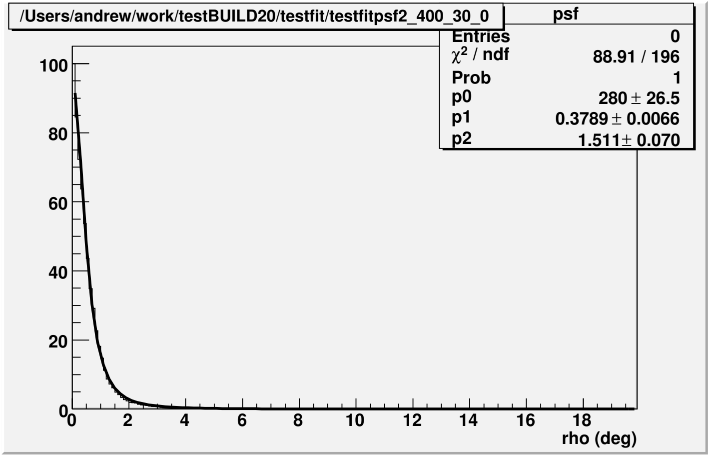

Point spread dispersion

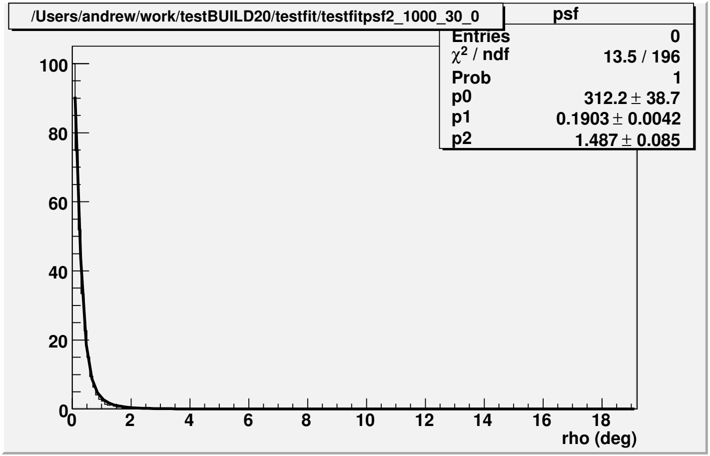

Physical sources - Effective area

- Physical sources are modeled as a sum of monoenergetic sources
- In principle, $A_{eff} = \frac{\sum_i A(E_i) w(E_i)}{\sum_i w(E_i)}$ where $w(E_i) = (E_{i+1}^{-\alpha} - E_i^{-\alpha}) \sum_j EDP(E_i, E_j)$ and all quantitites are a function of incidence angle in instrument coordinates, event type (G) and filter (FM)
- In practice, this quantity was too sensitive to small changes in the spectral index due to contributions from low energy photons, where the effective area is poorly calibrated.
- Therefore, we use $w(E_i) = f(E_i)(E_{i+1}^{-\alpha} - E_i^{-\alpha})$ where $f(E_i)$ is determined post-hoc

Physical sources - Point spread dispersion

- $PSD = \frac{\sum_i PSD(E_i)w(E_i)}{\sum_i w(E_i)}$ where $w(E_i) = (E_{i+1}^{-\alpha} - E_i^{-\alpha}) \sum_j A_{eff}(E_i)EDP(E_i, E_j)$ and all quantitites are a function of incidence angle in instrument coordinates, event type (G) and filter (FM)
- The current version (I0007/I0010) of the PSD files uses histograms taken directly from the Monte Carlo simulations. New PSD files (I0023/I0024) are in preparation which contain values derived from a fit to the Monte Carlo data using a three parameter King function:
- $f(\rho)d\Omega = N(1 - 1/\gamma)(1 + \frac{(\rho/\delta)^2)}{2\gamma})d\Omega$

In-flight Calibration Procedure

- Long-term integrations of AGILE in-flight data in both pointing (2007/07/13 - 2009/10/15) and spinning (2009/11/04 - 2010/10/31) modes of the Vela and anti-center regions, generating counts and exposure maps with a bin size of 0.3°
- Maximum likelihood analysis taking into account Galactic diffuse emission and isotropic background
- Point sources: Vela pulsar in the Vela region, Crab and Geminga pulsars and IC443 in the anti-center region
- Analysis performed with fixed position and fixed, power-law spectra
- Model counts compared to data to validate point spread function
- Spectra and fluxes compared to those published in the Fermi Catalog in order to determine the post-hoc scaling factors for the effective area

Energy-dependent effective area scaling factors

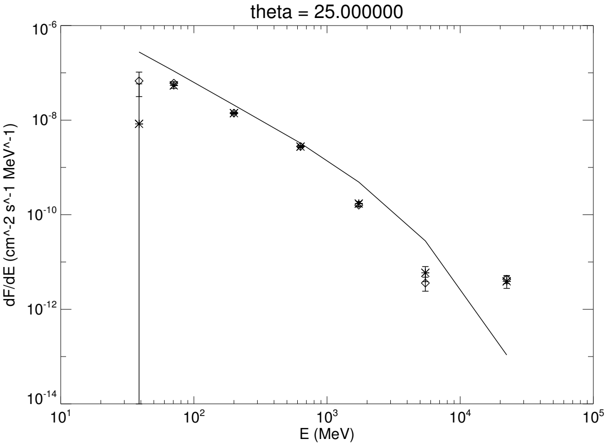

Figure: We introduce energy-dependent scaling factors into the sensitive area response function to correct for the underestimate of the flux and spectra. (I0023 → I0024)

Energy-dependent effective area scaling factors

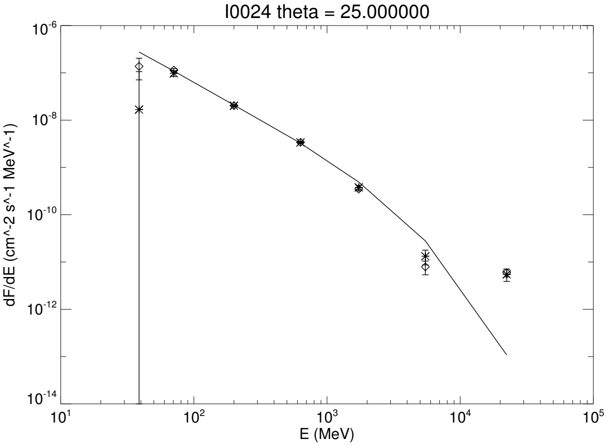

Figure: We introduce energy-dependent scaling factors into the sensitive area response function to correct for the underestimate of the flux and spectra. (I0023 → I0024)

Point spread function, Vela, $E > 100$ MeV

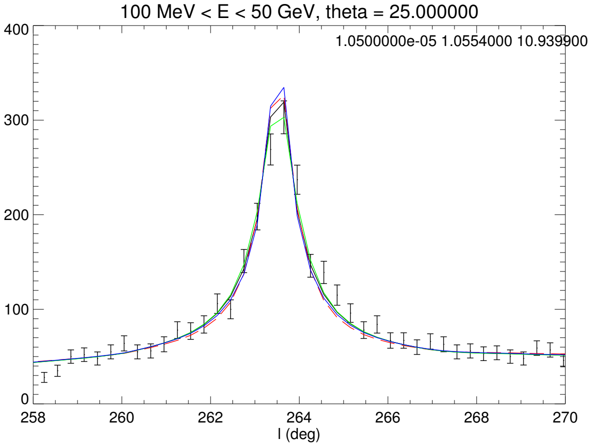

Figure: A 10° slice centered on Vela. The data are well-fit by the point-spread function assuming a spectral index of -1.66, weighted by effective area, spectrum, and energy dispersion.

Point spread function, Vela, $E > 100$ MeV

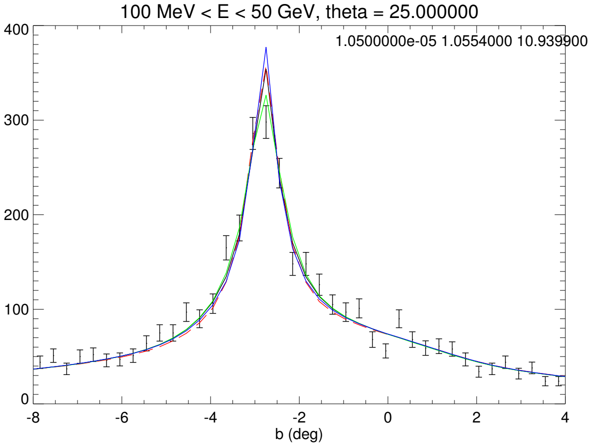

Figure: A 10° slice centered on Vela. The data are well-fit by the point-spread function assuming a spectral index of -1.66, weighted by effective area, spectrum, and energy dispersion.

Point spread function, Vela, $E > 400$ MeV

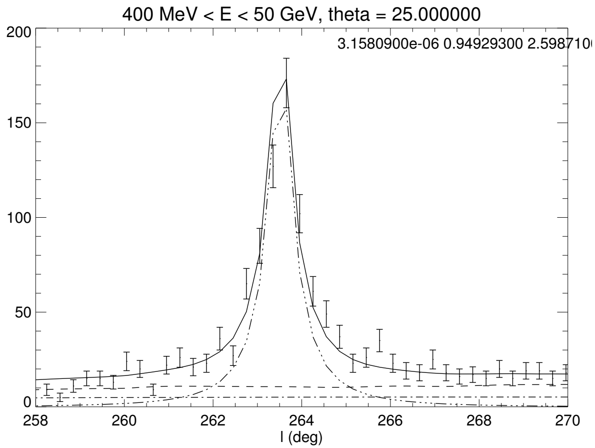

Figure: A 10° slice centered on Vela. The data are well-fit by the point-spread function assuming a spectral index of -1.66, weighted by effective area, spectrum, and energy dispersion.

Point spread function, Vela, $E > 400$ MeV

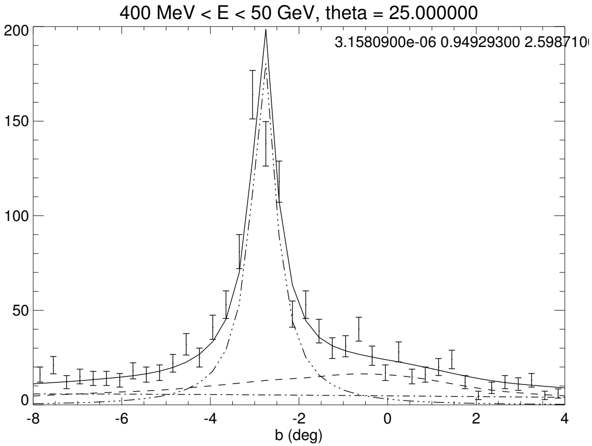

Figure: A 10° slice centered on Vela. The data are well-fit by the point-spread function assuming a spectral index of -1.66, weighted by effective area, spectrum, and energy dispersion.

Single energy vs. composite PSF

Energy (MeV)	68% C.R.
100	4.4°
400	1.35°
1000	0.69°

Table: 68% Containment radius, off-axis angle $= 30^\circ$, single energy

Energy Range	68% C.R.
100 MeV - 50 GeV	2.1°
400 MeV - 50 GeV	1.1°
1000 MeV - 50 GeV	0.8°

Table: 68% Containment radius, off-axis angle $= 30^\circ$, $\alpha = -1.66$

Work in progress

- Validate Crab flux and spectra, other sources
- Understand post-hoc scaling factors
- Allow AGILE-GRID scientific analysis below 100 MeV
- Re-evaluate EDP-dependent effective area calculation

Cross-calibration with Fermi - in preparation

- AGILE-GRID sensitivity is highest around 100 MeV, decreases rapidly above 10 GeV
- Fermi-LAT effective area is highest above 1 GeV, decreases rapidly below 200 MeV
- Use Fermi-LAT catalog data to determine how source flux below 200 MeV can change AGILE sensitivity for a give Fermi flux and spectrum
- In collaboration with Fermi, use simultaneous data to determine how energy dispersion, energy dependence of effective area, and off-axis exposure influence Fermi and AGILE sensitivity

AGILE & Fermi, 1-day exposure

	AGILE-GRID (pointing)	AGILE-GRID (spinning)	Fermi-LAT (front)
FOV (sr)	2.5	2.5	2.5
Rate of drift	$\approx 1^\circ/\text{day}$	$\approx 1^\circ/\text{sec}$	$\approx 4^\circ/\text{min}$
Sky coverage	1/5	$\approx$ 70%	whole sky
Source livetime fraction	≈ 0.5	≈ 0.2	≈ 0.16
1-day exposure (10^7 cm^2 s) 30° off-axis, 100 MeV	≈ 2	0.5-1	1-2

Fermi vs. AGILE pointing

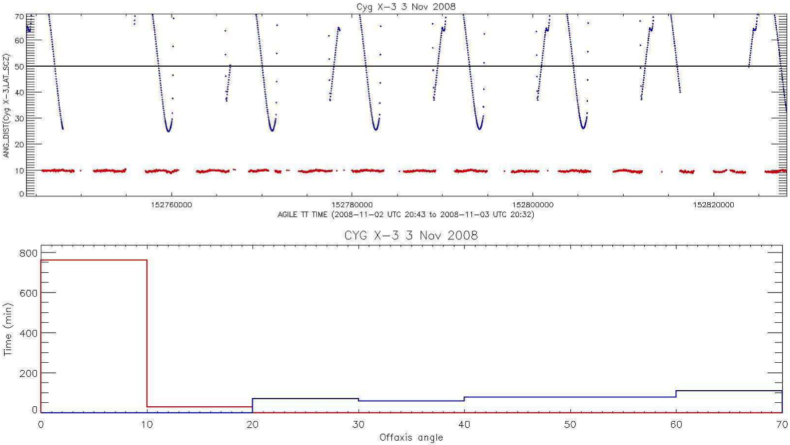

Figure: Top: off-axis angle vs. time; Bottom: histogram of off-axis angle. AGILE = red, Fermi = blue

Fermi vs. AGILE spinning

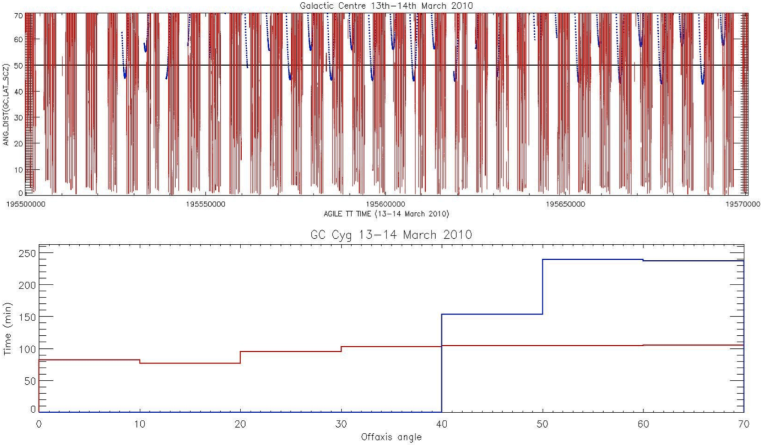

Figure: Top: off-axis angle vs. time; Bottom: histogram of off-axis angle. AGILE = red, Fermi = blue

Conclusion

- In-flight data confirm modeling of point spread function
- Extreme sensitivity to source spectrum due to large energy dispersion
- Post-hoc scaling factors compensate for lack of energy dispersion term in effective area calculation
  - More pronounced at lower and higher energies
- Necessary first step in cross-calibration with Fermi-LAT
- Many avenues to resolve apparent discrepancies